JOURNAL OF RAMAN SPECTROSCOPY
J. Raman Spectrosc. 2007; **38**: 647–659
Published online 30 April 2007 in Wiley InterScience
(www.interscience.wiley.com) DOI: 10.1002/jrs.1723

JRS

Low wavenumber Raman scattering of nanoparticles and nanocomposite materials

M. Ivanda,[1]* K. Furić,[1] S. Musić,[1] M. Ristić,[1] M. Gotić,[1] D. Ristić,[1] A. M. Tonejc,[2] I. Djerdj,[2] M. Mattarelli,[3] M. Montagna,[3] F. Rossi,[3] M. Ferrari,[4] A. Chiasera,[4] Y. Jestin,[4] G. C. Righini,[5] W. Kiefer[6] and R. R. Gonçalves[7]

[1] Ruđer Bošković Institute, Bijenička 54, 10000 Zagreb, Croatia
[2] Faculty of Sciences, Department of Physics, University of Zagreb, 10001 Zagreb, Croatia
[3] Dipartimento di Fisica, Università di Trento, CSMFO group, via Sommarive 14, I-38050 Povo, Trento, Italy
[4] CNR-IFN Istituto di Fotonica e Nanotecnologie, CSMFO group, via Sommarie 14, I-38050 Povo, Trento, Italy
[5] CNR-IFAC Nello Carrara Institute of Applied Physics, Lab. of Optoelectronic Technologies, Via Madonna del Piano 10, 50019 Sesto Fiorentino, Firenze, Italy
[6] Institut für Physikalische Chemie, Universität Würzburg, Am Hubland, D-97074 Würzburg, Germany
[7] Departamento de Química, Universidade de São Paulo, 14040-901 Ribeirão Preto – SP, Brazil

Received 15 November 2006; Accepted 19 January 2007

Low wavenumber Raman scattering of the acoustic vibrational modes of nanoparticles was used for the determination of the size distribution of free dielectric and semiconductor nanoparticles and of nanoparticles embedded in matrices. The theoretical background as well as the experimental results for the free noninteracting nanoparticles and for the nanoparticles in strong interaction with a surrounding matrix is described. The approach is based on a $1/\nu$ dependence of the Raman light-to-vibration coupling coefficient and on the fact that each nanocrystallite of diameter D vibrates with its eigenfrequency $\nu \sim 1/D$. The model calculation considers the inhomogeneous broadening due to contribution from the particles of different sizes, and homogeneous broadening due to interaction of particles with the matrix. The comparison of the calculated and experimental low wavenumber Raman spectra are presented for SnO_2, TiO_2 and CdS free nanoparticles and TiO_2, CdS_xSe_{1-x} and HfO_2 nanoparticles embedded in a glass matrix. The particle-size distributions determined by Raman scattering were compared to those found by TEM measurements. Raman spectroscopy proved to be a simple, fast and reliable method for size-distribution measurements. By an inverse procedure, starting from the Raman spectra and known particle-size distribution, a new method for the determination of the mean sound velocities of longitudinal and transverse phonons of nanoparticles is described. Copyright © 2007 John Wiley & Sons, Ltd.

KEYWORDS: low wavenumber Raman scattering; size distribution; nanoparticles; nanocomposite materials; longitudinal; transverse; sound velocity; SnO_2; TiO_2; CdS; HfO_2; hafnia; titania

INTRODUCTION

Nanoparticles and nanocomposite materials have attracted strong interest for their important physical and chemical properties. The main properties of these materials are related to the confinement of (quasi) particles (electrons, holes, excitons, phonons, etc.) in volumes with radii less than 10 nm. For this reason, the critical need for different applications of these materials is to have an accurate knowledge of the mean particle size and size distribution. The best and probably the most reliable technique for the determination of these quantities is transmission electron microscopy (TEM). Unfortunately, this technique is time consuming and needs expensive electron microscopes. The second most commonly used technique is X-ray scattering, where the Debye–Scherer equation is used for the determination of the particle size. This method is precise for the case of very narrow size distributions, but for broad distributions the systematic error could be more than 50%. To overcome this problem, it is necessary to include the complicated method of deconvolution of size distribution from the line profile and subtraction of the possible strain effects, and usually this procedure does not give a single solution.

*Correspondence to: M. Ivanda, Ruđer Bošković Institute, Bijenicka 54, 10000 Zagreb, Croatia. E-mail: ivanda@irb.hr

Raman scattering is one of the most important non-destructive techniques providing information on the vibrational and electronic states in a confined system. The problem of the vibrations of a spherical elastic body was solved by Lamb more than 100 years ago.[1] The low wavenumber Raman scattering (LWRS) from spherical acoustic vibrations of nanoparticles was first observed by Duval *et al*.[2] and, thereafter, LWRS has been used for the determination of the size of dielectric, semiconductor and metal nanoparticles embedded in glass[3–11] as well as of free nanoparticles.[12–17] Here we present a model for the calculation of the size distribution of nanoparticles from the line shape of the acoustic Raman peak. We also demonstrate how to apply this model for the determination of longitudinal and transverse sound velocities in nanoparticles when the size distribution is known.

THEORETICAL BACKGROUND

Raman spectroscopy is recognized as a powerful technique for the characterization of different nanostructures. Particles of nanometric size show low wavenumber vibrational modes that can be observed by Raman spectroscopy. These modes are of acoustic nature, involving the collective motion of large numbers of atoms and can be described by the elasticity theory of a continuum medium.[2] A century ago, Lamb[1] analyzed the vibrational spectrum of homogeneous elastic spherical particles and found that all frequencies scale with the inverse of their diameter. Recently, this theory was extended to consider various effects: shape effect, matrix effect, surface relaxation effects, etc.[3–17] Two types of modes, spheroidal and torsional, were found. The modes are classified according to the symmetry group of the sphere by the labels (l, m) as for the spherical harmonic function Y_{lm}. The angular number $l = 0, 1, 2, \ldots$ measures the number of wavelengths along a circle on the surface of the particle. Each mode l is $(2l + 1)$ times degenerate. These degenerate modes are labeled by the number m. Another index $p = 1, 2, 3, \ldots$ distinguishes the lowest-frequency mode, $p = 1$ (surface mode), of an (l, m) sequence from the $p = 2, 3, \ldots$ (internal modes) in increasing order of frequency. It has been shown[3] that the Raman scattering intensity of the $p = 2$ mode is only few percent of the $p = 1$ mode and the intensity further decreases with increasing p. The $l = 0$ spheroidal modes are purely radial with spherical symmetry. Duval[18] has shown that only the $l = 0$ and $l = 2$ spheroidal modes are Raman active. The $l = 0$ vibrations give polarized (VV) Raman spectra, whereas the $l = 2$ vibrations give depolarized spectra, contributing to the VV and HV spectra. The depolarization ratio, I_{HV}/I_{VV}, of the $l = 2$ vibrations and the relative Raman activities of the $l = 0$ and $l = 2$ spheroidal modes are system dependent and are related to the microscopic mechanism of electron–phonon coupling.[19–21] The wavenumbers of these modes ν_l^p are reciprocal to the particle diameter D,[2,3] i.e. $\nu_l{}^p = \beta_l{}^p/D$, where

$$\beta_l^p = \frac{S_l \mathrm{v}_l}{c} \tag{1}$$

Here v_0 and v_2 are the longitudinal and transverse velocities of sound, respectively, c is the vacuum light velocity, and $S_0{}^p$ and $S_2{}^p$ are constants, of the order of unity for the surface $(p = 1)$ mode and which depend on the ratio of the longitudinal and transverse velocities of sound within the particle as well as on the boundary conditions of the particle. The Raman spectrum of spatially confined vibrations is generally described by the Shuker and Gammon relation[22]

$$I_l(\nu, T) = \frac{n(\nu, T) + 1}{\nu} C_l(\nu) g(\nu) \tag{2}$$

where $C_l(\nu)$ is the light-to-vibration coupling coefficient, $g(\nu)$ is the density of vibrational states, T is the temperature, and $n(\nu, T) + 1$ is the Bose–Einstein occupation factor for the Stokes component.

In the model of Raman scattering on free noninteracting particles, $C(\nu)$ corresponds to the coupling of light with the particle frequency mode ν, and $g(\nu)$ represents the number of particles that vibrate with that frequency. To obtain the particle-size distribution from the experimental Raman line shape, the important question is of the dependence of the Raman light-to-vibration coupling coefficient on the particle size. Theoretically, it has been shown that for dielectrics in the off-resonance condition, the light-to-vibration coupling coefficient is proportional to the particle diameter and is consequently reciprocal[3] of the particle frequency, $C(\nu) \sim D \sim \nu^{-1}$. The vibrational lifetime of free (noninteracting particles) is expected to be relatively long and, therefore, the contribution of each particle mode to the broadening of each particle peak can be considered negligible. Therefore, for the $l = 0$ or $l = 2$ and as regards the surface $p = 1$ modes, the particle-size distribution $N(D)$ corresponds to the density of vibrational states $g(\nu)$ by using a simple substitution of ν with the corresponding diameter $D = \beta_l/\nu$:

$$N(D) \sim g(\nu) = \frac{I_l(\nu)^* \nu^2}{n(\nu) + 1} \tag{3}$$

where $I_l(\nu)$ is its Raman intensity. The density of vibrational states, $g(\nu)$, corresponds to the size distribution $N(D)$, since each particle vibrates with a frequency that is inversely proportional to its diameter D. The distribution of small particles (of nanometric size) is usually well approximated with a lognormal size distribution

$$N(D) \propto \exp\left[-\frac{(\ln(D/D_0)^2}{2\sigma^2}\right] \tag{4}$$

Here, D_0 is the diameter that corresponds to the maximum of the distribution and the parameter σ measures the

DOI: 10.1002/jrs

distribution width. The distribution of larger nanoparticles is usually better described with a Gaussian distribution:

$$N(D) \propto \exp\left[-\frac{(D-D_0)^2}{2\sigma^2}\right] \quad (5)$$

For the case of nanoparticles embedded in an elastic matrix, the vibrational modes are broadened owing to the interaction with the matrix and $C_l(\nu)$ is no more a sharp function of frequency. The origin of the broadening is in the shortening of the vibrational lifetime due to the fast transfer of the vibrational energy into the surrounding matrix. This effect is known as *homogeneous line broadening*. The homogeneous line shape $C_l(\nu)$ can be calculated if the densities, and the longitudinal and transverse sound velocities of the nanoparticle and the matrix are known.[3] In this case, the Raman scattering intensity, $I(\nu)$, for an ensemble of nanoparticles with the size distribution $N(D)$ is given by the integral of the homogeneously broadened Raman spectrum over the inhomogeneous distribution:

$$I_l^R(\nu) = \frac{n(\nu)+1}{\nu}\int C_l(\nu, D)N(D)dD \quad (6)$$

EXPERIMENTAL

Raman scattering experiments were carried out at room temperature with the argon ion 514.5 nm laser excitation line in backscattering configuration using a DILOR Z-24 triple monochromator. A special design of laser focusing[23] to the line probe of 2×0.05 mm^2 is used. In this way, a low laser irradiation of 30 W/cm^2, which avoids any significant local heating of the sample, is used. A krypton ion laser with the excitation line at 647 nm was used for the Raman excitation providing the off-resonance scattering condition of CdS_xSe_{1-x} samples. High-resolution transmission electron microscopy (HRTEM) measurements were performed by using a JEOL JEM 2010, 200 kV microscope with the point resolution of 0.19 nm. Dark-field micrographs at a magnification of 100 000× and HRTEM images at magnification of 300 000× and 600 000× were used for the determination of the particle-size distributions.

RESULTS

Raman scattering on acoustical modes of free SnO_2 nanoparticles

Tin dioxide (SnO_2) and SnO_2-based ceramics find various applications as gas sensors, catalysts, electrode materials, etc. The properties of these oxides, such as particle size and morphology, structural and physical properties and crystallinity, greatly depend on the method of their synthesis. Very fine and uniform SnO_2 particles were produced by slow hydrolysis of 0.384 M aqueous $SnCl_4$ solutions at room temperature for a long period of 10 years and, thereafter, by autoclaving of mother liquor at 160 °C for 24 h.

Figure 1 shows TEM images of the prepared sample. At higher magnification it is evident that the particles are of regular shape and well separated. Figure 2 shows the Raman spectrum of SnO_2 powder. Low wavenumber modes are those below 100 cm^{-1}. In the process of evaluation of the size distribution from the shape of LWR peaks, the most difficult problem is determining the background signal. Usually the background is a slow, wavenumber-dependent function caused by different processes such as quasielastic light scattering, electronic scattering, photoluminescence, etc. We found that the function $A\omega^x$ describes well the background in various types of free nanoparticles. Inset (a) in Fig. 2 shows the Raman spectrum in log–log coordinates. The straight line here is the estimated background with the $A\omega^x$ form. The low wavenumber part of the spectrum, after the subtraction of the background, is shown in inset (b) of Fig. 2. The main peak at 39.6 cm^{-1} is attributed to the symmetric vibrations, and the weaker peak at 18.2 cm^{-1} is attributed to the quadrupolar vibrations. The ratio of the wavenumber of these modes is

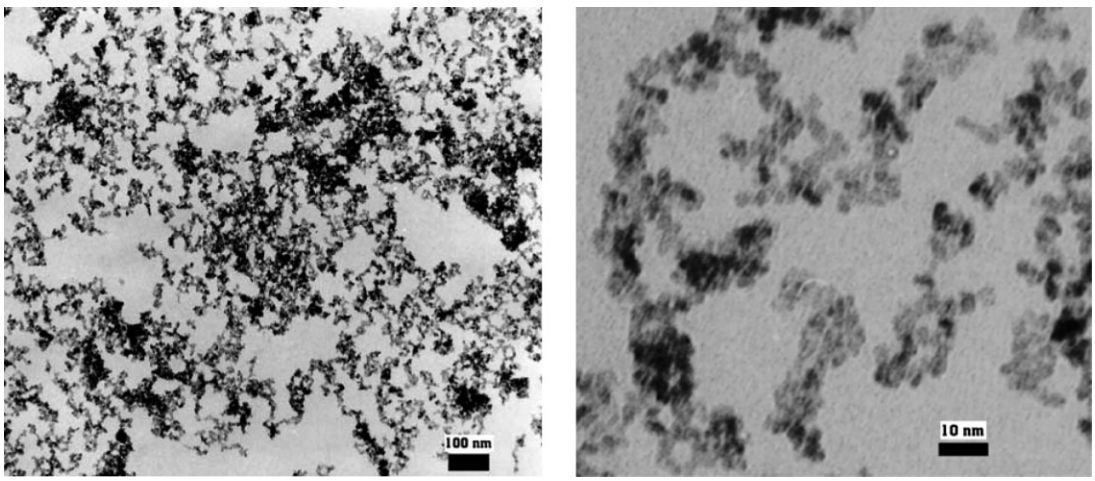

Figure 1. TEM images of SnO_2 nanoparticles at two different magnifications.

DOI: 10.1002/jrs

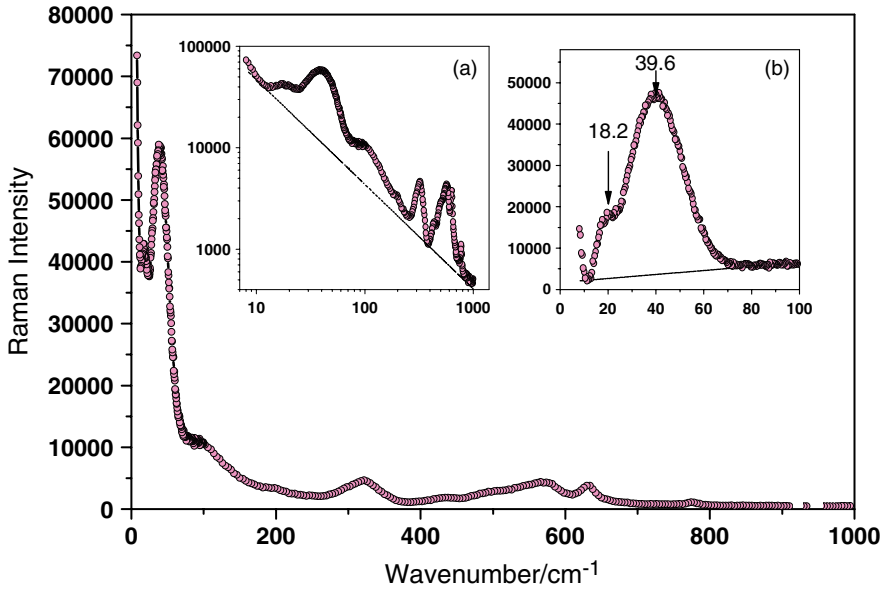

Figure 2. Raman spectrum of SnO_2 nanoparticles; inset (a) shows the Raman spectrum in log-log coordinates with estimated background; inset (b) shows the low wavenumber part of the Raman spectrum (circles). The line approximately separates the contribution of the surface mode from a further background mainly attributed to inner modes. This figure is available in colour online at www.interscience.wiley.com/journal/jrs.

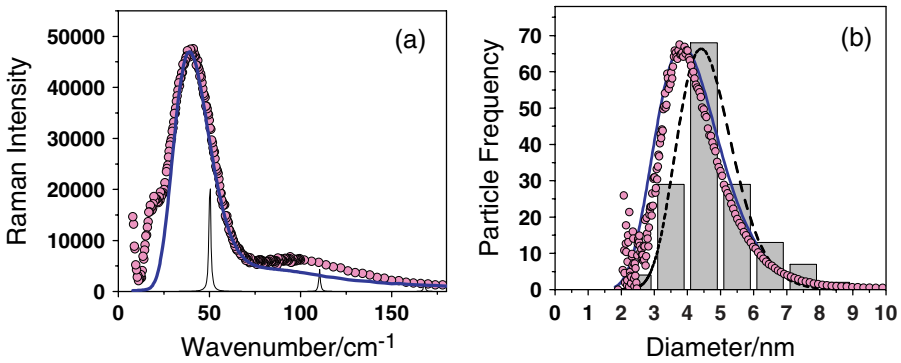

Figure 3. (a) Low wavenumber Raman spectrum of SnO_2. The tick line shows the calculated Raman spectrum for the $l = 0$ mode assuming inhomogeneous broadening caused by a log-normal size distribution with $D_0 = 3.85$ nm and $\sigma = 0.27$. The calculated spectrum for a single particle of diameter $D_0 = 3.85$ nm is also shown (thin line, sharp peaks that correspond to $p = 1$ and $p = 2$ modes). (b) comparison of size distributions: bars – TEM distribution, dashed line – log-normal function fitted on TEM distribution, bold line – distribution used for the fit of the previous Raman spectrum, circles – distribution found from the Raman spectrum directly. This figure is available in colour online at www.interscience.wiley.com/journal/jrs.

2.18. The symmetric mode should appear only in the VV polarized spectrum, whereas the quadrupolar mode should appear both in VV an VH spectra. However, the spectra of our powder sample are not polarized, the depolarization ratio being $I_{VH}/I_{VV} \sim 1$ at all wavenumbers. We explain this effect by multiple reflection of the laser beam and scattered Raman light between nanoparticles, where the information on polarization is lost, and for this reason the polarized Raman spectra could not be used for the assignment of these modes. The assignment of the two peaks to the symmetric and quadrupolar modes is based here on the comparison of the observed wavenumber ratio with the calculated value. The sound velocities of the SnO_2 crystal calculated as a mean value across four (for v_l) and seven (for v_t) crystalline sound propagating vectors are $v_l = 6530$ m/s and $v_t = 3120$ m/s, respectively.[24] Using the ratio $v_l/v_t = 2.09$, the coefficients S_0 and S_2 are obtained. Then, the parameters β_l calculated by Eqn (1) for the $l = 0$ and $l = 2$ modes are 1.94×10^{-5} and 0.87×10^{-5}, respectively. Therefore, the expected ratio for the wavenumbers of these modes is $\nu_0/\nu_2 = \beta_0/\beta_2 = 2.2$, which agrees well with the observed value.

Figure 3(a) shows the calculated spectrum of the $l = 0$ mode (bold line) obtained by using Eqn (6) with a $C(\nu) \sim D \sim \nu^{-1}$. The best fit was obtained for a lognormal distribution

DOI: 10.1002/jrs

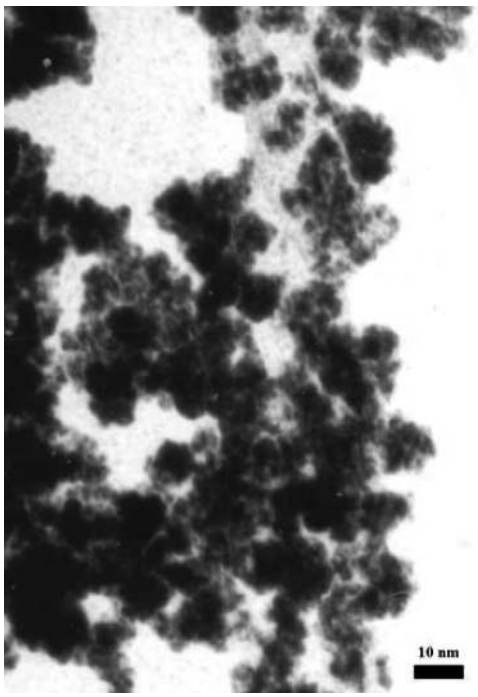

Figure 4. TEM image of CdS nanoparticles.

with $D_0 = 3.85$ nm and $\sigma = 0.25$, which were the only free parameters. The calculated spectrum reproduces well the shape of the main peak at about 40 cm^{-1}, attributed to the $l = 0$ surface vibrations. The experimental peak at about 100 cm^{-1}, which at first sight could be attributed to the $p = 2$ internal mode, is not reproduced by the calculation, which gives very broad and not-well-resolved $p = 2$, 3 contributions. On the other hand, the peak at about 100 cm^{-1} was found on a number of SnO_2 samples of different mean particle sizes and, therefore, could not be ascribed to the particle modes. It could be due to Raman scattering at the edge of the Brillouin zone or to vibrational modes induced by disorder that became Raman active owing to the breakdown of selection rules, such as local lattice imperfections and oxygen deficiencies.

The calculated Raman spectrum, i.e. $C(\nu)/\nu^2$ for the particle size of 3.85 nm, with the sharp peaks of $p = 1$ and $p = 2$ modes, is also shown in Fig. 3(a) (thin line). It is evident that the maximum of the inhomogeneously broadened peak is shifted by ~20% toward low wavenumbers in comparison to the sharp peak of the $p = 1$ mode of a single particle. This shows that Eqn (1) gives reliable values of the particle size only when the size distribution is sharp. In the presence of a wide size distribution, a correction is needed because big particles scatter more than small particles: the size obtained by Eqn (1) with the maximum of the LWR peak is larger than the mean size of the distribution and the difference is as high as the distribution is broad.

Figure 3(b) shows the comparison of the size distributions obtained by Raman and TEM data. Two size distributions, obtained by the shape of the Raman spectrum, are shown. The first (bold line) is the lognormal distribution used for the fit shown in Fig. 3(a). The second distribution (circles) has been obtained directly from the Raman spectrum by the

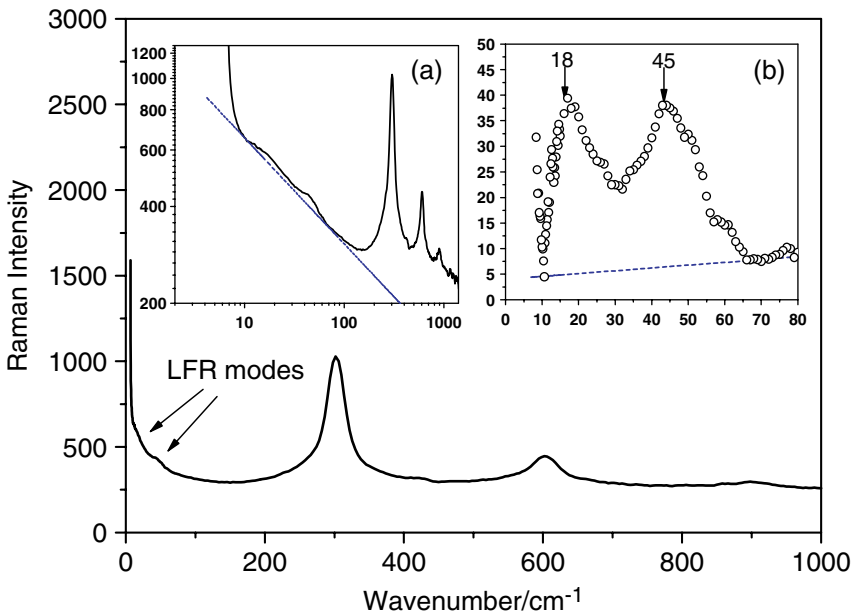

Figure 5. Raman spectrum of CdS nanoparticles: inset (a) shows the Raman spectrum in log–log coordinates with estimated background; inset (b) shows the low wavenumber part of Raman spectrum with subtracted background. The position of symmetric and quadrupolar modes are indicated by arrows. This figure is available in colour online at www.interscience.wiley.com/journal/jrs.

DOI: 10.1002/jrs

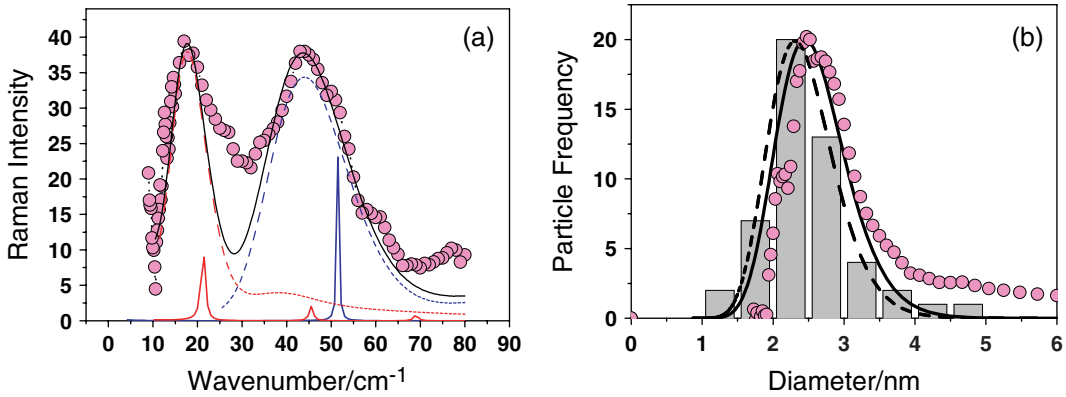

Figure 6. (a) Experimental Raman spectrum of CdS powders after the subtraction of the background (circles). Calculated Raman spectra of the $l = 0$ (dashed line) and $l = 2$ (dotted line) modes are by using a lognormal size distribution with $D_0 = 2.45$ nm and $\sigma = 0.195$. Sum of the $l = 0$ and $l = 2$ calculated spectra (solid line). The calculated spectrum for a single particle of $D_0 = 2.45$ nm is also shown (sharp peaks of $p = 1$ and $p = 2$ modes); (b) Comparison of the size distributions obtained by TEM (bars), lognormal fit of TEM data (dashed line), lognormal used for the fit of Fig. 6(a), where D_o and σ are the fittings parameters only, distribution found from the Raman spectrum directly, having attributed the whole spectrum to symmetric modes (circles). This figure is available in colour online at www.interscience.wiley.com/journal/jrs.

following procedure:

1. After subtraction of the $A\omega^x$ background in log–log coordinates (where A and x are free parameters), the LWRS signal is further corrected by subtraction of a linear background below two neighboring minima of the LWR peak (see inset (b) in Fig. 2). This correction is mainly for the subtraction of the contribution of the inner modes ($p = 2, 3, 4 \ldots$) of the symmetric peak.
2. The resulting spectrum $I(\nu)$ is further divided by the Bose–Einstein occupation factor $(n(\nu) + 1)$ and multiplied by ν^2 (approximately multiplied by ν^3, because at low frequencies $1/(n(\nu) + 1) \sim \nu$).
3. The final step is to replace the frequency ν with the corresponding particle diameter $D = \beta/\nu$. The resulting function then represents the particle-size distribution (circles in Fig. 3(b))

This simple procedure gives a size distribution very close to the lognormal distribution obtained by the fit of the Raman spectrum, even without need of subtracting the contribution of the quadrupolar mode, which is weak and superimposed on the symmetric contribution on the low wavenumber side, where the ν^3 factor further reduces its importance. Finally, the size distribution obtained by TEM is well reproduced by a lognormal curve, but it is sharper ($\sigma^{\mathrm{TEM}} = 0.19$, $\sigma^{\mathrm{RAMAN}} = 0.27$) and has a larger mean size ($D_0{}^{\mathrm{TEM}} = 4.4$ nm, $D_0{}^{\mathrm{RAMAN}} = 3.85$ nm). We ascribe the difference mainly to the error in size distribution determined by TEM.[17]

Raman scattering of acoustical modes of free CdS nanoparticles

The CdS nanoparticles were prepared by the sol–gel process. Figure 4 shows the TEM images of a powder sample. Figure 5 shows the Raman spectrum of the same sample.

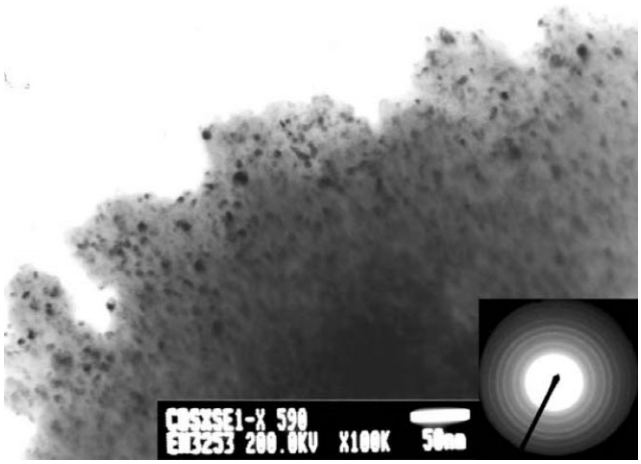

Figure 7. TEM image of the sample OG 590 with CdS_xSe_{1-x} nanocrystals.

The low wavenumber particle modes are indicated by arrows. Inset (a) in Fig. 5 shows the Raman spectrum in log–log coordinates. Here we used again the power function $A\omega^x$, which best describes the background of the powder sample containing free nanoparticles. The low wavenumber spectrum with subtracted background is shown in inset (b) of Fig. 5. Two peaks are observed here: one at 45 cm^{-1} attributed to the symmetric surface mode, and the other at 18 cm^{-1}, attributed to the quadrupolar surface mode. The wavenumber ratio of these modes is 2.5.

We can compare it with the calculated one. The parameters β_l are calculated using $v_l = 4250$ m/s, $v_t = 1860$ m/s and $\rho = 4.87$ g/cm^3 for CdS.[25] Using the ratio $v_l/v_t = 2.28$, the coefficients S_0 and S_2 are obtained. Then, the parameter β_l calculated by Eqn (1), for the $l = 0$ and $l = 2$ modes is 1.29×10^{-5} and 0.52×10^{-5}, respectively. Therefore,

DOI: 10.1002/jrs

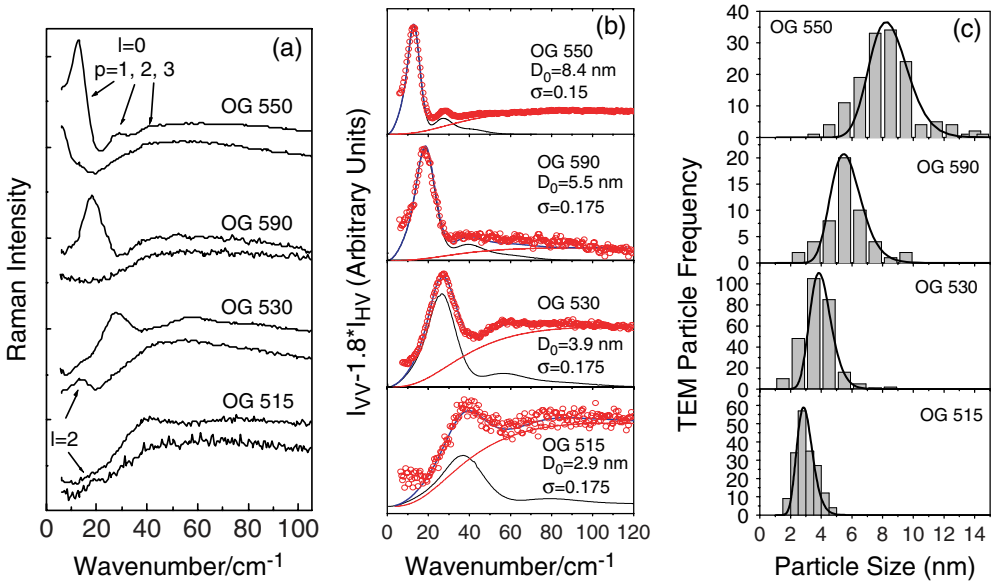

Figure 8. (a) Low wavenumber VV (upper) and HV (bottom) polarized Raman spectra of different Schott glasses (the p sequence of the $l = 0$ symmetric mode is labeled). For the samples with smaller particle diameters, OG 530 and OG 515, the $l = 2$ mode is also observable; (b) The $I_{VV} - 1.8 \times I_{HV}$ spectra (circles) fitted with the boson peak (broad background signal) and CdS_xSe_{1-x} symmetric mode (solid line), which is homogeneously and inhomogeneously broadened owing to the interaction of the nanocrystals with the glass matrix and to the particles size distributions, respectively. The sum of these contributions is shown by the thick solid line that fits the experimental spectrum. D_0 and σ are the parameters of the used lognormal distribution. (c) Comparison of size distributions obtained by TEM (bars) and those found from the Raman spectra (solid line). This figure is available in colour online at www.interscience.wiley.com/journal/jrs.

the expected ratio for the wavenumbers of these modes is $\beta_0/\beta_2 = 2.42$, which agrees well with the observed value.

Figure 6(a) shows the calculated spectra of the symmetric (dashed line) and quadrupolar (dotted line) modes. A lognormal size distribution with $D_{0v} = 2.45$ nm and $\sigma = 0.195$ gives the best fit. Apart for the overall intensity, a further free parameter was the relative scattering efficiency of the two modes, which was taken in order to have an overall good agreement between the experimental and the weighted sum of the $l = 0$ and $l = 2$ calculated spectra (bold line). Figure 6(b) shows a comparison of the size distributions obtained by TEM and Raman spectra, by the methods described in detail for the case of SnO_2 nanoparticles. Note that the whole spectrum, after the further subtraction of the background shown in the inset (b) of Fig. 5, has been used for the direct determination of the size distribution (circuits). The peak at about 18 cm^{-1} on the same inset, due to the $l = 2$ modes, would have been subtracted for this calculation, since the method derives the size distribution from the shape of the $l = 0$ surface peak. Anyway, the $l = 2$ contribution is not very important even in this case, in which its peak has intensity in the Raman spectrum similar to that of the $l = 0$ peak. This is because of the already discussed ν^3 factor. Anyway, the large tail of the calculated distribution, which shows a weak structure around 4.5 nm, is the spurious effect of the missed subtraction of the $l = 2$ contribution. The agreement between the size distributions obtained by TEM and Raman is excellent: they have the same width ($\sigma = 0.195$) and are quite close to the values of the maxima ($D_0{}^{TEM} = 2.3$ nm, $D_0{}^{RAMAN} = 2.45$ nm).

The main difference between the experimental and calculated Raman spectrum of Fig. 6(a) is in the range between the symmetric and quadrupolar mode peaks. A possible explanation is that modes other than the $l = 0$ and $l = 2$ spheroidal ones could appear in the Raman spectrum. This is forbidden for the spherical particles, but not for the particles of low symmetry, where the (l, m) labels will lose the full meaning. In particular, vibrations that resemble the $l = 1$ torsional mode of a sphere are expected to have a wavenumber intermediate between those of the $l = 2$ and $l = 0$ spheroidal mode and could contribute to the Raman spectrum of a very distorted particle. Figure 4 shows that the CdS particles have more irregular shape than the SnO_2 particles of Fig. 1.

LWRS of CdS_xSe_{1-x} nanoparticles in a glass matrix

The increased interest for these materials started with the discovery of their saturable absorption that promises their use as a Q-switching element in lasers.[26] With large nonlinear optical properties[27] as well as a fast response time,[28] the material could possibly have interesting application in waveguides,[29] optical switches[30] and bistable resonators.[28] A critical need for the application in all these fields of nonlinear optics is to accurately know the mean particle size and size distribution.

DOI: 10.1002/jrs

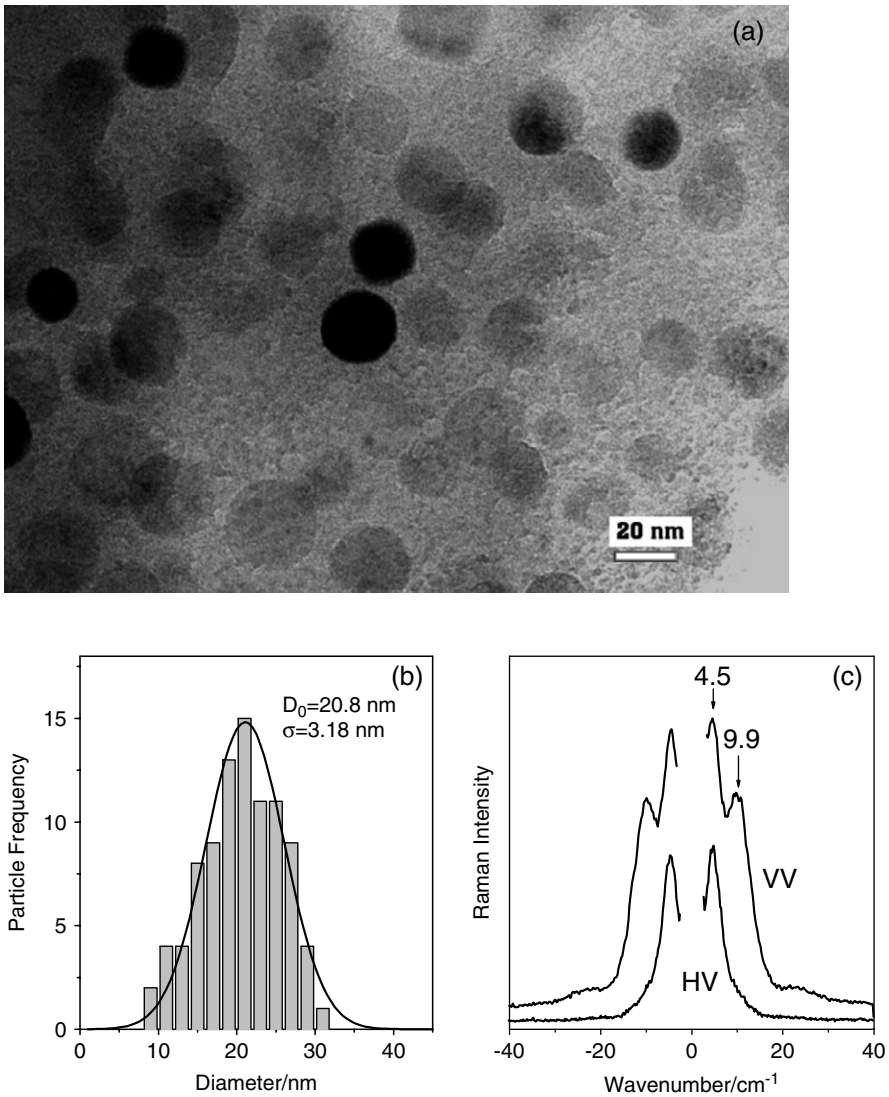

Figure 9. (a) TEM image of a sol–gel $0.8SiO_2-0.2TiO_2$ film heated at 1300 °C showing anatase crystals in a glass matrix; (b) size distribution of these crystals and its fit by a Gaussian function with mean size $D_0 = 20.8$ nm and $\sigma = 3.18$ nm; (c) Stokes and anti-Stokes LWR spectra of the glass–ceramic film.

The commercially available Schott filter glasses with different concentrations of CdS_xSe_{1-x} quantum dots of different sizes, in particular OG515, OG530, OG550 and OG590, were investigated by means of LWRS. The numbers next to the letters indicate the cut-off wavelength in nanometers of the glass. Figure 7 shows TEM image of the sample OG 590, where CdS_xSe_{1-x} crystals appear as dark spots. Figure 8(a) shows the low wavenumber VV and HV polarized Raman spectra of the acoustical vibrations of the CdS_xSe_{1-x} particles in a glass matrix. Both types of modes, symmetric and quadrupolar, appear in the polarized VV spectra. Together with the symmetric surface mode ($p = 1$), the symmetric inner modes ($p = 2, 3$) are also observable in the spectra. The quadrupolar mode ($l = 2$) is depolarized and clearly observed in the HV polarized spectra. All modes are superimposed on the 'boson peak'[31] – a broad signal that is a common feature for most glasses (here with a maximum near 50 cm^{-1}), and the quasielastic scattering peak (QES)[32] that appears below 30 cm^{-1}. In order to remove the contribution of QES peak, the HV polarized spectra were divided by the depolarization ratio of QES, $\rho_{QES} = 5/9$ ($\rho = I_{HV}/I_{VV}$) as measured on our samples, and then subtracted from the VV polarized Raman spectra. We note here that the quadrupolar mode is depolarized and, therefore, its contribution is mainly cancelled by this procedure. The resulting spectra $VV - 1.8 \times HV$, shown in Fig. 8(b), consist of the $l = 0$ symmetric mode, its inner radial modes ($p = 2, 3, \ldots$) and of the remaining contribution of the boson peak, which has a depolarization ratio higher than that of QES. The phenomenological function, const. $\times \nu^3 (40^2 + \nu^2)^{-1}$.,[7] was used to fit the boson peak on all spectra with the boson peak intensity as a free parameter.

DOI: 10.1002/jrs

The LWR line shape is caused by both inhomogeneous and homogeneous broadening. The former is directly related to the size distribution $N(D)$. The homogeneous line shape may be calculated if the densities, and the longitudinal and transverse sound velocities of the nanocrystals and of the surrounding medium are known. The Raman spectra of the symmetric surface and inner modes were fitted with Eqn (6) using the lognormal distribution. The results of the fit (D_0 and σ) are shown on Fig. 8(b). The parameters β are calculated using $v_l = 3690$ m/s, $v_t = 1620$ m/s and $\rho = 5.66$ g/cm^3 for CdSe and $v_l = 4250$ m/s, $v_t = 1860$ m/s and $\rho = 4.87$ g/cm^3 for CdS.[25] For the glass matrix we used the values of silica glass: $v_l = 5960$ m/s, $v_t = 3790$ m/s and $\rho = 2.3$ g/cm^3. The shape of the homogeneous profile does not change very much with the content parameter x, from pure CdS to pure CdSe. The homogeneous and inhomogeneous broadenings have comparable effects on the actual linewidth of the surface ($p = 1$) mode. Figure 8(c) shows very good agreement between the particle-size distributions obtained by TEM and Raman measurements.

Raman scattering from acoustical modes of TiO_2 nanoparticles embedded in a glass matrix

SiO_2–TiO_2 is an important glassy system for many applications, in particular for planar waveguides, because of the easy tunability of the refractive index and low losses.[33] The glass is not stable, and TiO_2 crystals nucleate and grow after thermal annealing at temperatures around 900 °C. Therefore, crystallization occurs before or together with densification by thermal annealing in sol–gel-derived glasses, at least for relatively high TiO_2 contents (>20%). $SiO_2(1-x)$–$TiO_2(x)$ films, with x in the range 0.07–0.2, were deposited on silica substrates by a dip-coating technique. The starting solution was obtained by mixing tetraethylorthosilicate (TEOS), ethanol, deionized water and hydrochloric acid as a catalyst. Titanium isopropoxide (TiPOT) was used as the TiO_2 precursor.

The TEM image of a sample $SiO_2(0.8)$–$TiO_2(0.2)$ annealed at 1300 °C for 30 min is shown on Fig. 9(a). The spherical particles are crystals with the anatase structure. The size distribution obtained from Fig. 9(a) and its fit with a Gaussian function are shown in Fig. 9(b). The Stokes and anti-Stokes VV and HV polarized Raman spectra of these nanocrystals are shown in Fig. 9(c). In the VV spectrum both $l = 0$ and $l = 2$ spheroidal modes are visible, whereas only the quadrupolar mode is visible in the HV spectrum.

As for the above-discussed case of CdS nanocrystals in glasses, the LFRS peaks of anatase are also affected by homogeneous and inhomogeneous broadening. Here we demonstrate how to apply this model for the determination of longitudinal and transverse sound velocities in nanoparticles when the size distribution is known. The procedure is self consistent and converges very fast, even in two steps:

1. The homogeneously broadened $C(\nu)$ for anatase TiO_2 in silica is calculated by using the sound velocities of the most symilar structure, here of rutile;
2. The such determined $C(\nu)$ is than used to fit the VV and HV Raman spectra. In this way, the first approximate values of the constants β_l, S_l and of the sound velocities of anatase are determined.

The procedure is repeated with these new sound velocities. The starting sound velocities of rutile calculated as a mean value across 11 (for v_l) and 9 (for v_t) crystalline sound propagating vectors are: $v_l = 9017$ m/s and $v_t = 5394$ m/s. Using the ratio $v_l/v_t = 1.672$, the coefficients S_0 and S_2 are found by the methods of Ref. 3, and the parameter β calculated for the $l = 0$ and $l = 2$ modes are 2.39×10^{-5} and 1.51×10^{-5}. After three recursive steps of the above procedure a good convergence for the anatase is achieved. The fit gives $\beta_0 = 2.66 \times 10^{-5}$, $\beta_2 = 1.10 \times 10^{-5}$, $v_l = 8880$ m/s, $v_t = 3900$ m/s and $v_l/v_t = 2.27$, implying an average sound velocity of 4400 m/s, which is larger than that found for the anatase from the heat capacity measurements (3560 m/s).[34]

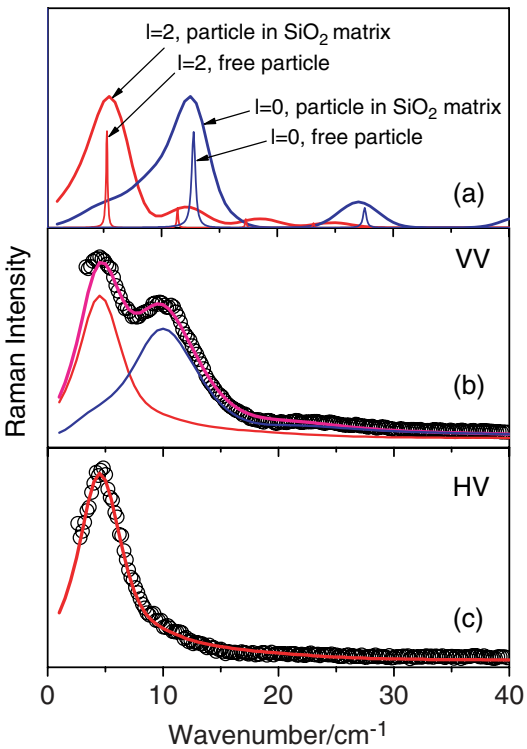

Figure 10. (a) calculated symmetric and quadrupolar Raman peaks of the free anatase particle of 20.8 nm diameter (sharp lines) and of the same particle in SiO_2 matrix (solid lines); (b) fit of the symmetric and quadrupolar modes on the VV polarized Raman spectrum with the size distribution obtained from the TEM; (c) the same fit for the quadrupolar mode in the HV Raman spectrum. This figure is available in colour online at www.interscience.wiley.com/journal/jrs.

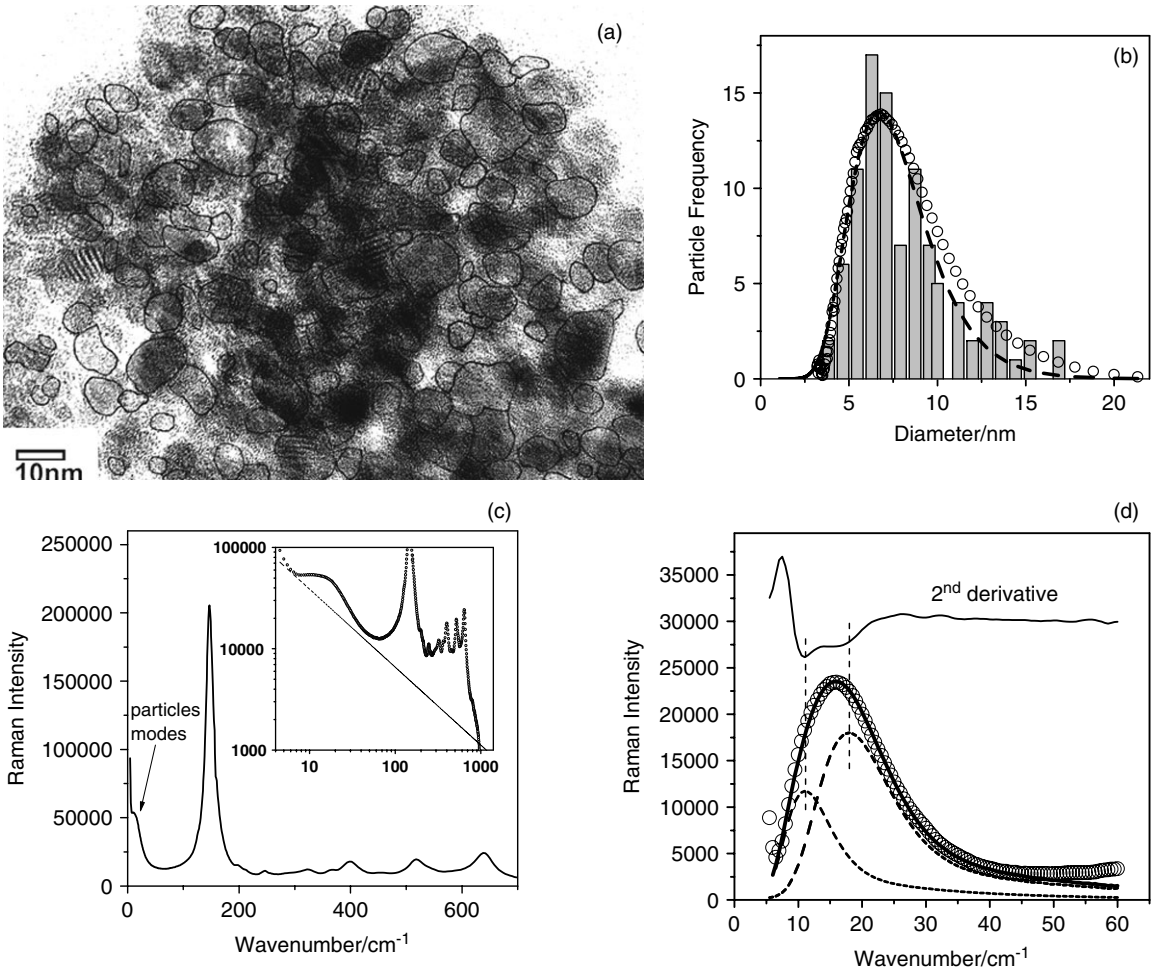

Figure 11. TiO_2 powder sample: (a) TEM image – the particles are artificially surrounded according to the observation of the crystalline planes; (b) particle-size distribution found by TEM (bars) with fitted lognormal distribution curve (dashed line) and distributions obtained directly from the Raman spectrum (circles); (c) Raman spectrum of anatase with indications of LFR particle modes, the inset showing the same spectrum in a log–log scale and the estimated background; (d) Raman spectrum after the subtraction of the estimated background (circles), calculated inhomogeneously broadened lineshape of the symmetric and quadrupolar mode (dashed lines), their sum (solid line) and the second derivative of the Raman spectrum.

Figure 10 shows the results of this self-consistent fitting procedure on the polarized LWR spectra. Figure 10(a) shows the results of the calculation for the symmetric and quadrupolar mode of a particle of 20.8 nm diameter, free (sharp peaks) and in a silica matrix (broad peaks). For the homogeneous line shape of the quadrupolar mode $C_2(\nu)$ we used that calculated for the symmetric mode, scaled to the frequency of the quadrupolar mode. Figure 10(b) and (c) show the results of the fit of the VV and HV polarized Raman spectra by using the size distribution measured by TEM. The fit gives a depolarization ratio for the quadrupolar mode $\rho_2 = 1$ and for the symmetric mode $\rho_0 = 0$.

Raman scattering from acoustical modes of free TiO_2 nanoparticles

The samples of nanosized TiO_2 powder particles (free nanoparticles) were synthesized by the sol–gel procedure based on the hydrolysis of Ti(IV)-isopropoxide under different experimental conditions. The sample labeled here as S2 was thermally treated for 1 h at 350 °C in a nitrogen atmosphere.

Figure 11(a) shows the TEM image of this sample. A broad distribution of sizes is observed. Furthermore, most TiO_2 nanoparticles have a shape quite different from the spherical one. Figure 11(b) shows the size distribution derived from the TEM image (bars) and its fit with the a lognormal function (dashed line). Figure 11(c) shows the Raman spectrum of the sample S2. The LWR modes are superimposed on the laser line tail on one side and to the tail of the E_g band at 145 cm^{-1} of the anatase phase on the other side, plus an unknown background signal. Therefore, for the signal under the particle peak (total background signal) we use again the $A\omega^x$ wavenumber dependence, which passes through the minima on both sides of the peak (dashed line on

DOI: 10.1002/jrs

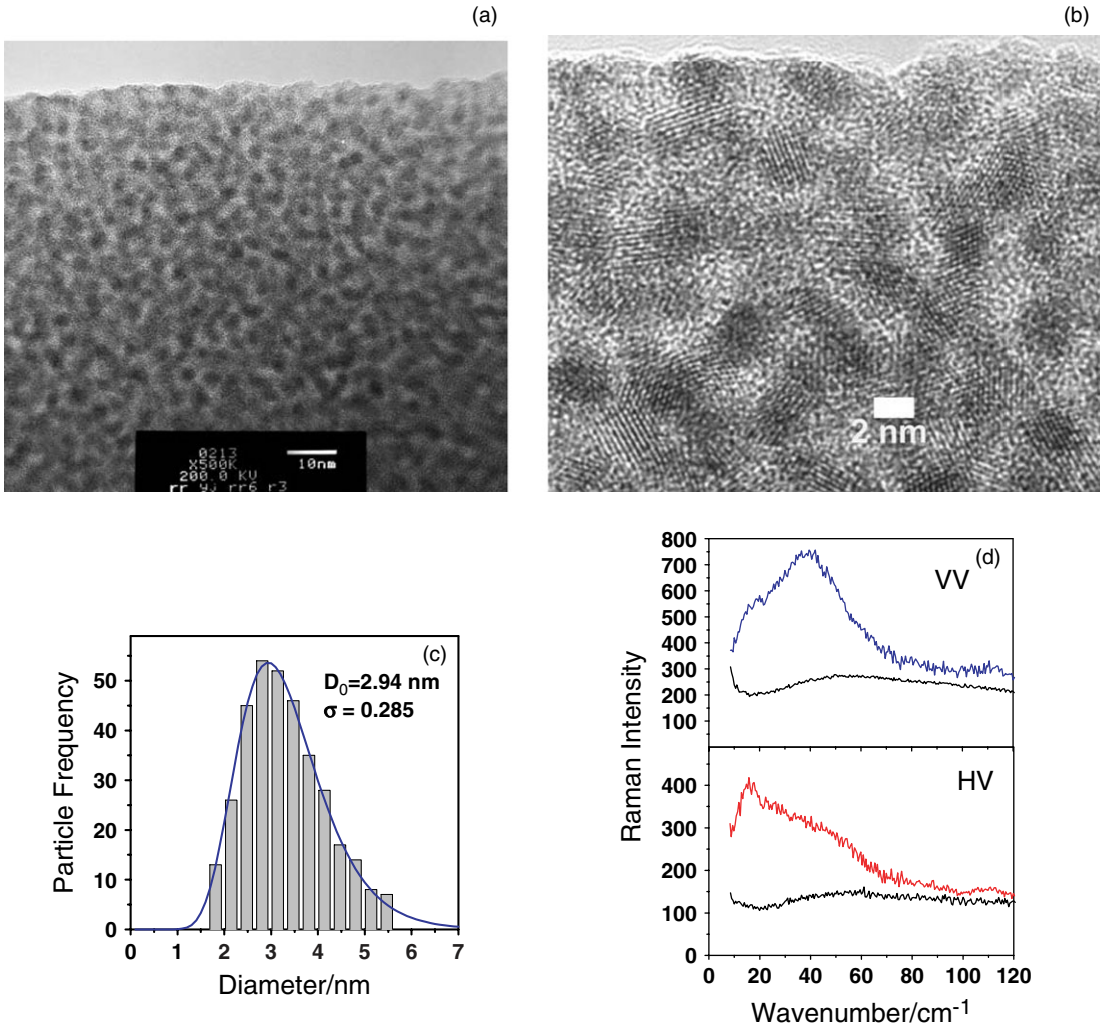

Figure 12. (a) TEM image of a sol–gel $0.7SiO_2$–$0.3HfO_2$ film heated at 1000 °C showing HfO_2 crystals in a glass matrix; (b) magnified part of the (a) with visible crystalline planes of nanoparticles; (c) size distribution of the crystals and its fit by a lognormal function; (d) VV and HV polarized Raman spectra, obtained by exciting at 457.9 nm in the TE_0 mode of the waveguide for the glass-ceramic annealed at 1000 °C (upper spectra) and for the glass annealed at 900 °C (lower spectra). This figure is available in colour online at www.interscience.wiley.com/journal/jrs.

the inset of Fig. 11(c)). The Raman spectrum with subtracted background is shown in Fig. 11(d). Here, the strong multiple scattering in the powder sample fully depolarizes the exciting laser light, thereby avoiding the opportunity to separate the VV and HV spectra. Therefore, the observed broad peak cannot be easily attributed to vibrational modes of a defined symmetry. If the whole spectrum is attributed to a single (l, m, p), the size distribution can be extracted directly from the Raman spectrum. By using $\beta = 1.69 \times 10^{-5}$, the best agreement with the TEM distribution is obtained, as shown in Fig. 11(b) (circles). The obtained β-value is in the range of $\beta = (1.59 \pm 0.14) \times 10^{-5}$ found on 14 different TiO_2 powder samples,[17] assuming that only quadrupolar vibrations are active in the Raman spectra of TiO_2 nanoparticles. The fact that the calculated size distribution is broader than that observed by TEM (see Fig. 11(b)), together with the observation that anatase nanoparticles in a glass matrix show both $l = 0$ and $l = 2$ modes with comparable intensities, suggests that a more detailed analysis is needed.

Figure 11(d) shows a tentative fit of the particle peak with two contributions obtained by calculating the shapes of two Raman peaks of free particles with a lognormal ($D_0 = 6.7$ nm and $\sigma = 0.31$) size distribution found from the fit of TEM distribution and with both β_l constant and peak intensities as free parameters. The positions of the resulting peaks from the fit are also confirmed by the second derivative of the Raman spectrum. The obtained parameters for β_l are 1.78×10^{-5} and 1.10×10^{-5}. The second one corresponds to the $l = 2$ mode of the anatase phase, but the first cannot be ascribed to the $l = 0$ mode, which should have $\beta_0 = 2.66 \times 10^{-5}$. It is possible that modes other than the $l = 2$ and $l = 0$ modes, in particular the $l = 1$ (torsional) mode with an intermediate wavenumber,

due to the very irregular shape of the anatase nanocrystals shown in Fig. 1 could cause the breaking of the selection rules. A further effect should be considered for particles with important distortion from the spherical shape: the five m components of the $l = 2$ mode are no more degenerate and a further source of peak broadening is present.[35] Because of all the above difficulties, a definitive attribution of the observed scattering in TiO_2 powders is not possible at present.

Sound velocities in hafnia determined by LWRS

Hafnia (HfO_2) is technologically important because of its extraordinarily high bulk modulus, high melting point and high chemical stability, as well as its high neutron absorption cross-section. HfO_2 resembles its twin oxide, zirconia (ZrO_2), in many physical and chemical properties. Several films of $(0.7)SiO_2-(0.3)HfO_2$ were prepared by a sol–gel dip-coating technique.[36]

The TEM image of a sample annealed at 1000 °C for 30 min is shown in Fig. 12(a) and a part of this image at a higher magnification in Fig. 12(b). The size distribution determined from TEM and fitted by a lognormal function with parameters $D_0 = 2.94$ nm and $\sigma = 0.285$ is shown in Fig. 12(c). The Stokes VV and HV polarized Raman spectra of these nanocrystals are shown in Fig. 12(d). In the VV spectrum both $l = 0$ and $l = 2$ spherical modes are visible.

Here, as for the case of anatase particles in silica matrix, we used the self-consistent fitting procedure for the determination of sound velocities in hafnia. We started again with the coupling coefficient $C(\nu)$ of rutile in silica matrix, and after three steps the procedure converged with the results shown in Fig. 13.

Figure 13(a) shows the calculated symmetric and quadrupolar Raman peaks for a free hafnia particle of 2.94 nm diameter (sharp peaks) and for the hafnia particle in a silica matrix (broad peaks). For the coupling coefficient function of the quadrupolar mode $C_2(\nu)$ we used again the value calculated for the symmetric mode, which is then scaled to the wavenumber of the quadrupolar mode. Figures 13(b) and (c) show the results of a self-consistent fit to the symmetric and quadrupolar modes in the VV and HV polarized Raman spectra using Eqn (6) with the known size distribution from the TEM measurements. The

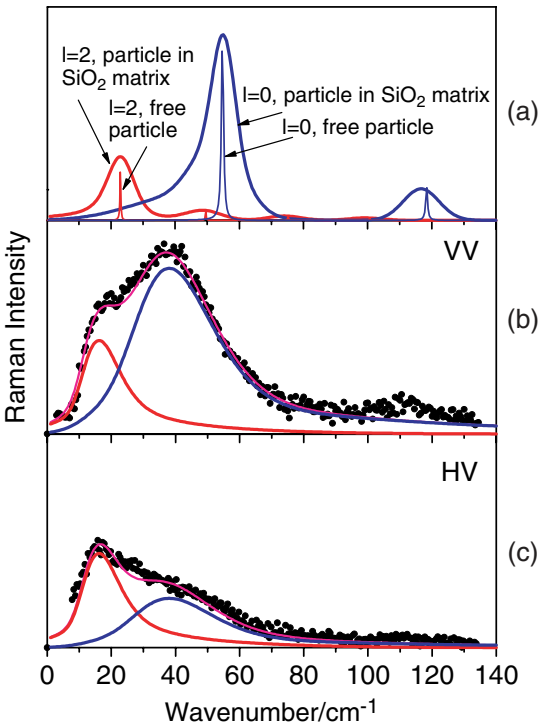

Figure 13. (a) Calculated symmetric and quadrupolar Raman peaks of the free hafnia particle of 2.94 nm diameter (sharp lines) and of the same particle in a SiO_2 matrix (solid lines); (b) fit of the symmetric and quadrupolar modes on the VV polarized Raman spectrum using the size distribution from TEM measurements; (c) the same fit for the quadrupolar mode in HV Raman spectrum. This figure is available in colour online at www.interscience.wiley.com/journal/jrs.

resulting parameter β_l and sound velocities for hafnia are $\beta_0 = 1.62 \times 10^{-5}$ and $\beta_2 = 0.68 \times 10^{-5}$, $v_l = 5405$ m/s and $v_t = 2410$ m/s. The appearance of the symmetric mode in HV polarization could be due to multiple reflections of the excitation and scattered light. In contrast to the powder samples, because of the lower density of particles here, this effect is smaller.

A rough estimation of the mean sound velocities of the tetragonal HfO_2 is obtained by scaling for the square root of the density the sound velocities of ZrO_2, indeed

Table 1. A summary of the results for the calculation and LWRS determination of the parameters β_l and sound velocities

	v_l (m/s)	v_t (m/s)	$\rho g/(cm)^3$	$\beta_l \times 10^7$	$\beta_t \times 10^7$	β_l/β_t (calc).	β_l/β_t (exp.)
SiO_2	5950	3760	2.26				
CdS	4250	1860	4.87	126	52	2.42	2.5
CdSe	3690	1620	5.66	112	46	2.43	2.5
SnO_2	6530	3120	6.994	194	88	2.20	2.18
TiO_2-rutile	9020	5390	4.25	239	151	1.56	
TiO_2-anatase (our values by LWRS)	8880	3900	3.8	266	110	2.41	2.2
HfO_2 (our values by LWRS)	5405	2410	9.33	162	68	2.39	2.41

DOI: 10.1002/jrs

assuming that the two systems have the same elastic constants.[37] Zirconia (ZrO_2) is surprisingly similar to hafnia (HfO_2) in many physical and chemical properties, owing to their homological electronic outer shell configuration. These compounds are hard ceramics with comparable high dielectric constants and wide band gaps. For the high-temperature cubic phases of HfO_2 and ZrO_2, the elastic constants have been calculated and they are practically identical for the two compounds.[38] The obtained values, $v_l = 5400$ m/s and $v_t = 3070$ m/s for the tetragonal phase, and $v_l = 5970$ m/s and $v_t = 3560$ m/s for the monoclinic phase, well compare with those obtained by the Raman-TEM procedure.

CONCLUSIONS

We have analyzed the acoustical modes in the Raman spectra of different nanocrystals and nanocomposite materials. The theory of Raman scattering from spherical vibrational modes was applied in order to calculate the size distribution of nanoparticles. For the free nanoparticles, the inhomogeneous broadening of the symmetric and quadrupolar Raman peaks was applied. For the nanoparticles embedded in a matrix, the homogeneous broadening due to the interaction of the particles with the matrix was also taken into account. A summary of results is presented in Table 1. The size distribution obtained from the Raman spectra shows good agreement with the TEM measurements. We show that an inverse approach, which uses the shape of the Raman peaks and the size distribution measured by TEM, allows the determination of the longitudinal and transverse sound velocities of the nanoparticles. This approach could be very important for the determination of the elastic properties of nanoparticles.

REFERENCES

1. Lamb H. *Proc. London Math. Soc.* 1882; **13**: 189.
2. Duval E, Boukenter A, Champagnon B. *Phys. Rev. Lett.* 1986; **56**: 7052.
3. Montagna M, Dusi R. *Phys. Rev., B* 1995; **52**: 10080.
4. Fujii M, Nagareda T, Hayashi S, Yamamoto K. *Phys. Rev., B* 1996; **54**: R8373.
5. Bischof T, Ivanda M, Lermann G, Materny A, Kiefer W. *J. Raman Spectrosc.* 1996; **27**: 297.
6. Saviot L, Champagnon B, Duval E, Kudriavtsev IA, Ekimov AI. *J. Non-Cryst. Solids* 1996; **197**: 238.
7. Saviot L, Champagnon B, Duval E, Ekimov AI. *Phys. Rev., B* 1998; **57**: 341.
8. Duval E, Portes H, Saviot L, Fuji M, Sumitomo K, Hayashi S. *Phys. Rev., B* 2001; **63**: 75405.
9. Ivanda M, Babocsi K, Dem C, Schmitt M, Montagna M, Kiefer W. *Phys. Rev., B* 2003; **67**: 235329.
10. Montagna M, Moser E, Visintainer F, Zampedri L, Ferrari M, Martucci A, Guglielmi M, Ivanda M. *Sol.-Gel Sci. Technol.* 2003; **26**: 241.
11. Saviot L, Murray DB, Marco de Lucas MC. *Phys. Rev., B* 2004; **69**: 113402.
12. Gotić M, Ivanda M, Sekulić A, Musić S, Popović S, Turković A, Furić K. *Mater. Lett.* 1996; **28**: 225.
13. Musić S, Gotić M, Ivanda M, Popović S, Turković A, Trojko R, Sekulić A, Furić K. *Mater. Sci. Engin., B* 1997; **47**: 33.
14. Ivanda M, Musić S, Popović S, Tonejc A, Gotić M. *J. Mol. Struct.* 1999; **480–481**: 645.
15. Ivanda M, Musić S, Gotić M, Turković A, Tonejc AM, Gamulin O. *J. Mol. Struct.* 1999; **480–481**: 641.
16. Ristic M, Ivanda M, Popovic S, Musić S. *J. Non-Cryst. Solids* 2002; **303**: 270.
17. Ivanda M, Tonejc AM, Djedj I, Gotić M, Musić S, Mariotto G, Montagna M. *Lecture Notes in Physics: Nanoscale Spectroscopy and Its Applications to Semiconductor Research*, Watanabe Y, Heun S, Salviati G, Yamamoto N (eds). Springer: Berlin, 2002; 16.
18. Duval E. *Phys. Rev., B* 1992; **46**: 5795.
19. Mattarelli M, Montagna M, Rossi F, Chiasera A, Ferrari M. *Phys. Rev., B* 2006; **74**: 153412.
20. Bachelier G, Mlayah A. *Phys. Rev., B* 2004; **69**: 205408.
21. Huntzinger JR, Mlayah A, Paillard V, Wellner A, Combe N, Bonafos C. *Phys. Rev.* 2006; **74**: 115308.
22. Shuker R, Gammon RW. *Phys. Rev. Lett.* 1970; **25**: 222.
23. Ivanda M, Furic K. *Appl. Opt.* 1992; **31**: 6371.
24. Rossler U, Strauch D, Madelung O, Schulz M. *Landolt-Bornstein, Semiconductors, Subvolume C*, vol. 41. Springer-Verlag: Berlin, 2003; 145.
25. Schultz M (ed.). The sound velocities were calculated as a mean value for different crystalline directions 1,5,7 for v_L and 2,3,4,5,6 v_T). *Semiconductors, Landolt-Bornstein, New Series*, vol. 4. Springer: New York, 1998.
26. Bret G, Gires F. *Appl. Phys. Lett.* 1964; **4**: 175.
27. Jain RK, Lind RC. *J. Opt. Soc. Am.* 1983; **73**: 647.
28. Yumoto J, Fukuskima S, Kubodera K. *Opt. Lett.* 1987; **12**: 832.
29. Ironside CN, Cullen TJ, Bhumbra BS, Bell J, Banyai WC, Finlayson N, Seaton CT, Stegeman GI. *J. Opt. Soc. Am. B* 1988; **5**: 492.
30. Najafi SI, Belanger M, Maciejko R, Black RJ. *Appl. Opt.* 1988; **27**: 806.
31. Ivanda M, Kiefer W, Mariotto G. *Solid State Commun.* 2001; **117**: 423.
32. Fontana A, Rossi F, Carini G, D'Angelo C, Tripodo G, Bartolotta A. *Phys. Rev. Lett.* 1997; **78**: 1078.
33. Tosello C, Rossi F, Ronchin S, Rolli R, Righini GC, Pozzi F, Pelli S, Fossi M, Moser E, Montagna M, Ferrari M, Duverger C, Chiappini A, De Bernardi C. *J. Non-Cryst. Solids* 2001; **284**: 230.
34. Dames C, Poudel B, Wang WZ, Huang JY, Ren ZF, Sun Y, Oh JI, Opeil C, Naughton MJ, Chen G. *Appl. Phys. Lett.* 2005; **87**: 031901.
35. Mariotto G, Montagna M, Viliani G, Duval E, Lefrant S, Rzepka E, Mai C. *Europhys. Lett.* 1988; **6**: 239.
36. Jestin Y, Afify N, Armellini C, Berneschi S, Bhaktha SNB, Boulard B, Chiappini A, Chiasera A, Dalba G, Duverger C, Ferrari M, Goyes Lopez CE, Mattarelli M, Montagna M, Moser E, Nunzi Conti G, Pelli S, Righini GC, Rocca F. *SPIE* 2006; **6183**: 438.
37. Kisi EH, Howard CJ. *J. Am. Ceram. Soc.* 1998; **81**: 1682.
38. Terki R, Feraoun H, Bertrand G, Aourag H. *Comput. Mater. Sci.* 2005; **33**: 44.